JOURNAL OF MATERIALS SCIENCE 24 (1989) 143–153

Cavitation and fracture in the superplastic Al–33% Cu eutectic alloy

ATUL H. CHOKSHI
Division of Materials Science and Engineering, Department of Mechanical Engineering, University of California, Davis, California 95616, USA

TERENCE G. LANGDON
Departments of Materials Science and Mechanical Engineering, University of Southern California, Los Angeles, California 90089–1453, USA

Experiments were conducted on the Al–33% Cu eutectic alloy in both an annealed and an as-extruded condition. For both conditions, the relationship between flow stress and strain rate is sigmoidal with maximum ductilities occurring at intermediate strain rates in the superplastic Region II. Specimens fail by necking at the faster strain rates in Region III, but the severity of necking is reduced with decreasing strain rate and the necks are very diffuse in Region II. There is extensive internal cavitation in the fractured specimens, especially at lower strain rates and in the vicinity of the fracture tip. It was observed that cavities form preferentially on the α-θ interphase boundaries. It is shown by calculation that the observed change from small rounded cavities to large cavities elongated along the tensile axis is reasonably consistent with the theories of cavity growth in fine-grained superplastic alloys

1. Introduction

Superplasticity refers to the ability of some materials to pull out to very high tensile elongations without failure. In early work, attention was devoted primarily towards the mechanical properties of superplastic materials and it was generally considered, as exemplified by a contemporary review [1], that internal cavities were not formed during superplastic deformation.

More recently, it has become firmly established that cavities are formed in many (if not most) superplastic alloys, and it is now generally recognized that cavity nucleation, growth and interlinkage are important parameters influencing both the total elongation to failure and the type of fracture. An analysis of the superplastic fracture processes [2] has led to two requirements for optimal superplasticity: (i) a suppression of localized (but not necessarily of diffuse) necking and (ii) a suppression of significant cavity interlinkage (but not necessarily of cavity nucleation and growth, since an array of stable cavities may co-exist in a material exhibiting a very large elongation to failure).

The Al–33% Cu eutectic alloy is a classic superplastic material which has been the subject of numerous investigations [3–34]. It is surprising to note, however, that there have been only four reports to date of cavitation in this material. In early investigations of the mechanical behaviour of this alloy, Petty [6] and Bright *et al.* [14] reported the formation of internal cavities on the α–θ interphase boundaries. More recently, Kashyap and Tangri [29, 31] noted the occurrence of cavitation in four specimens tested at strain rates from 10^{-5} to 10^{-2} sec^{-1}.

It is shown elsewhere [33, 34] that the mechanical properties of the Al–33% Cu eutectic alloy depend on the stability of the initial microstructure. When the alloy is tested in a well-annealed condition, there is no evidence for grain growth at low strains and the stress–strain curves rapidly attain a steady-state condition at low strain rates [33]; whereas when the alloy is tested in an as-extruded condition, the stress–strain curves show strain hardening at low strain rates due to concurrent grain growth [34]. These problems were not considered in the earlier reports of cavitation in this alloy, and in three cases the specimens were tested without a prior anneal and by heating up to and holding at the test temperature for short times ($\sim$40 min [14] and $\sim$45 min [29, 31], respectively) prior to starting the test.

This paper describes a detailed investigation of cavitation and fracture in the Al–33% Cu eutectic alloy using two separate sets of specimens in an annealed and an as-extruded condition, respectively. As will be shown, cavitation occurs under both conditions, but there are differences both in the extent of cavitation under any selected testing condition and in the total elongations to failure.

2. Experimental procedure

The Al–33% Cu alloy is a eutectic containing approximately equal volumes of a solid-solution Al–Cu α-phase and an intermetallic $CuAl_2$ θ-phase. The material was received in the form of extruded bars with a width of 280 mm and a thickness of 98 mm: details of the fabrication procedure were given previously [33]. A semi-quantitative spectrographic analysis revealed the following impurities in p.p.m.: silver 50 and calcium < 10.

0022–2461/89 $03.00 + .12

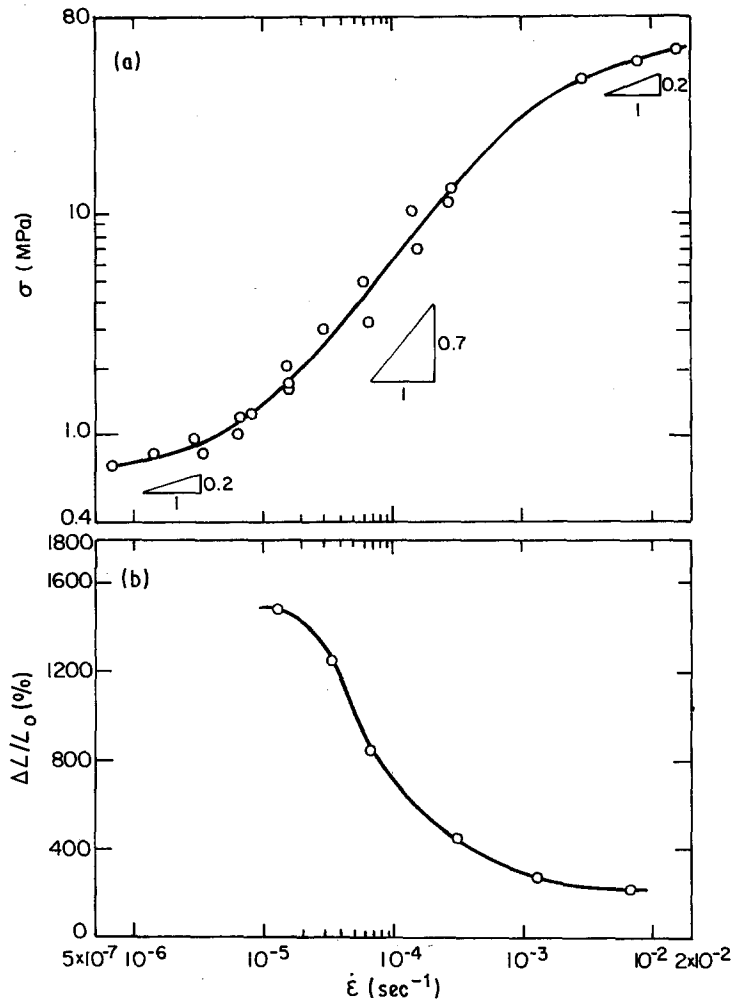

Figure 1 (a) Flow stress and (b) elongation to failure against strain rate for the annealed condition. $T = 723\,K$, $\bar{L} = 7.9\,\mu m$.

Cylindrical tensile specimens were machined from the bars with gauge lengths, parallel to the extrusion direction, of 6.4 mm for measurements of the total ductility or either 12.7 or 25.4 mm for measurements of the mechanical properties. All specimens were pulled in tension in air using an Instron testing machine operating at a constant rate of crosshead displacement. The tests were conducted at a temperature of 723 K using a long (~60 cm) split furnace with the temperature maintained constant to within ± 3 K over a central length of 10 cm within the furnace. The longer specimens were used to determine the relationship between the stress and strain rate, and the shortest specimens, with a gauge length of 6.4 mm, were pulled to failure, sectioned longitudinally, and then polished for microscopic examination using SiC papers, diamond paste and 0.3 μm alumina powder. Specimens were examined using both optical and scanning electron microscopy.

The tests were performed using specimens from two different batches of material and in either an annealed or an as-extruded condition.

For the first batch of material, the grains were elongated in the extrusion (tensile) direction by a factor of ~2 in the as-extruded condition. The linear intercept grain sizes were measured both parallel ($\bar{L}_1$) and perpendicular ($\bar{L}_2$) to the extrusion axis, and the average grain size was defined as $(\bar{L}_1 + \bar{L}_2)/2$. Almost all of the specimens from this batch of material were tested in an annealed condition after annealing for 16 h at a temperature of 793 K. The annealing treatment led to some grain growth and a more equiaxed grain configuration, as shown by the grain size measurements for Batch 1 in Table I.

All specimens from the second batch of material were tested in an as-extruded condition without a prior annealing treatment. These specimens also exhibited an initially elongated grain structure, and the values of the linear intercept grain sizes are given under Batch 2 in Table I.

3. Experimental results

3.1. Mechanical properties

Full details of the mechanical properties of this alloy are given elsewhere [33, 34]. For completion, the upper portions of Figs 1 and 2 show the variation of flow stress, σ, with the instantaneous strain rate, $\dot{\varepsilon}$, for the annealed ($\bar{L} = 7.9\,\mu m$) and as-extruded ($\bar{L} = 6.6\,\mu m$) conditions, respectively.*

For the annealed condition, the relationship between σ and $\dot{\varepsilon}$ is sigmoidal, with a maximum strain rate sensitivity $m = \partial(\ln \sigma)/\partial(\ln \dot{\varepsilon})$ of 0.7 at intermediate strain rates and a decrease to $m \simeq 0.2$ at both lower and higher strain rates. The region of high m at intermediate strain rates is usually termed Region II, and this is the region of maximum superplasticity because there is a correlation, both experimentally [35] and theoretically [36, 37], between the value of m and the

*Fig. 1 shows the steady-state flow stress for the annealed material, but in Fig. 2 for the as-extruded material, where steady-state behaviour was not achieved, the stresses were calculated at the strains where the loads reached the maximum values.

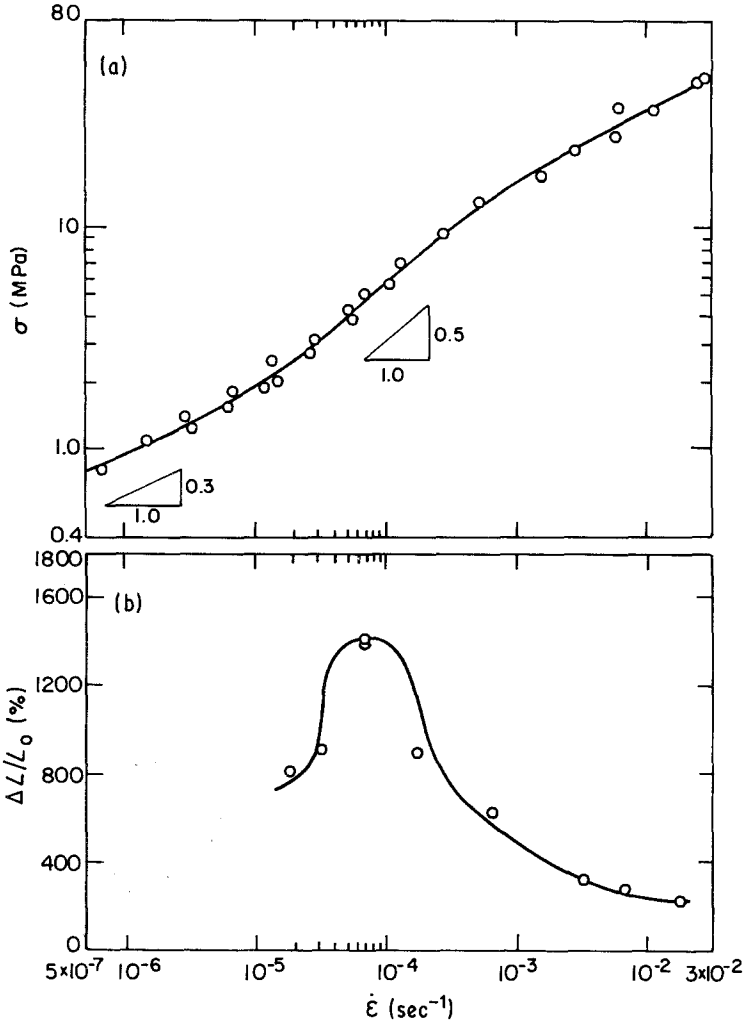

Figure 2 (a) Flow stress and (b) elongation to failure against strain rate for the as-extruded condition. $T = 723\,K$, $\bar{L} = 6.6\,\mu m$.

total elongation to failure. The regions of lower m at low and high strain rates are termed Regions I and III, respectively.

There is also a sigmoidal relationship between σ and $\dot{\varepsilon}$ in the as-extruded condition, with $m \simeq 0.5$ in Region II and $m \simeq 0.3$ in Region I.

There was no evidence for grain growth in the annealed condition, even at the lowest experimental strain rate of $6.7 \times 10^{-7}\,sec^{-1}$, so that the decrease in strain rate sensitivity in Region I represents the genuine behaviour of the material [33]. Although there was some minor grain growth in the as-extruded condition, calculations show that there is again a genuine Region I at low strain rates [34].

Using the specimens with the shortest gauge length, the lower portions of Figs 1 and 2 show the variation of the total elongation to failure, $\Delta L/L_0(\%)$, with the initial strain rate, where ΔL is the change in gauge length and L_0 is the initial gauge length. No tests were conducted at strain rates below $10^{-5}\,sec^{-1}$ because of the very long testing times required. Both curves show a transition from low elongations in Region III to very high elongations in Region II, with maximum elongations of the order of 1400% for both material conditions. A significant difference between the two sets of data is the subsequent decrease in elongations to failure in the as-extruded condition at strain rates below $\sim 5 \times 10^{-5}\,sec^{-1}$.

TABLE I Grain sizes for the annealed and as-extruded conditions

Material	Linear intercept grain size (μm)		
	$\bar{L}_1$	$\bar{L}_2$	$\bar{L}$
Batch 1			
As-extruded	6.6 ± 0.7	3.4 ± 0.2	5.0 ± 0.5
After annealing	8.7 ± 0.8	7.0 ± 0.9	7.9 ± 0.9
Batch 2			
As-extruded	7.8 ± 0.6	5.4 ± 0.4	6.6 ± 0.5

Fig. 3 shows several of the specimens after fracture in the as-extruded condition, where Specimen A is untested, Specimen B was tested at an initial strain rate of $1.3 \times 10^{-1}\,sec^{-1}$ to failure at 125%,* specimen C at $3.3 \times 10^{-2}\,sec^{-1}$ to 200%, Specimen D at $6.7 \times 10^{-3}\,sec^{-1}$ to 270%, Specimen E at $6.7 \times 10^{-4}\,sec^{-1}$ to 630%, Specimen F at $1.3 \times 10^{-4}\,sec^{-1}$ to 890%, Specimen G at $6.7 \times 10^{-5}\,sec^{-1}$ to 1400%, Specimen H at $3.3 \times 10^{-5}\,sec^{-1}$ to 890%, and Specimen I at $1.3 \times 10^{-5}\,sec^{-1}$ to 810%.

Inspection of Fig. 3 shows that at the highest strain rates in Region III specimens failed by the development of a sharp localized neck within the gauge length (Specimens B and C), but the neck becomes more diffuse as the strain rate is reduced towards Region II (for example, Specimen E). Under optimum superplastic conditions, the specimen pulls out in a fairly

*The datum point for Specimen B is not included in Fig. 2.

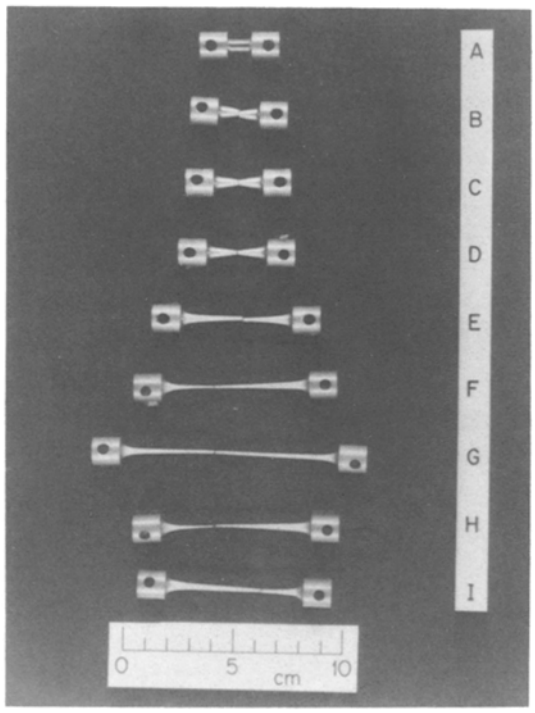

Figure 3 Specimens after fracture in the as-extruded condition: Specimen A is untested, and the other specimens were tested at initial strain rates of (B) $1.3 \times 10^{-1}\,sec^{-1}$, (C) $3.3 \times 10^{-2}\,sec^{-1}$, (D) $6.7 \times 10^{-3}\,sec^{-1}$, (E) $6.7 \times 10^{-4}\,sec^{-1}$, (F) $1.3 \times 10^{-4}\,sec^{-1}$, (G) $6.7 \times 10^{-5}\,sec^{-1}$, (H) $3.3 \times 10^{-5}\,sec^{-1}$ and (I) $1.3 \times 10^{-5}\,sec^{-1}$.

uniform manner and necking, if any, is very gradual (Specimen G). However, even under these optimal conditions, the specimen exhibits a reasonable cross-sectional area at the point of failure, and it does not pull out to a fine point as in some other superplastic alloys such as Zn–22% Al [38] and Pb–62% Sn [39]. At even lower strain rates towards Region I, there is again diffuse necking as the strain rate sensitivity decreases in value; inspection of Fig. 3 shows that Specimens F and H are very similar in appearance and they relate to regions on the stress–strain-rate curve having similar values of m.

3.2. The occurrence of cavitation

Several specimens were sectioned and examined for internal cavitation after failure, and it is useful to make some general comments concerning these observations.

First, for most specimens, and especially those tested at the higher strain rates, cavitation was a maximum in the vicinity of the fracture tip, and the total extent of cavitation tended to decrease with increasing distance from the fracture tip. In the following sections, a series of photomicrographs is presented both of the fracture tips and of areas which appeared to be reasonably representative of cavitation within the gauge length.

Second, all of the photomicrographs in this report are for specimens pulled to failure, and there was no attempt to investigate in detail the cavity configurations in any specimens prior to failure. However, it should be noted that, in connection with measurements of grain growth reported elsewhere for both the annealed and as-extruded condition [33, 34], several specimens were sectioned and optically examined at elongations of $< 40\%$ and there was no evidence for cavitation in any of these specimens. On the other hand, some cavities were visible in an as-extruded specimen from Batch 1 ($\bar{L} = 5.0\,\mu m$) pulled to an elongation of 135% at an initial strain rate of $1.7 \times 10^{-5}\,sec^{-1}$.

Photomicrographs are presented for three annealed specimens and four as-extruded specimens, as listed in Table II in terms of the initial strain rate, elongation to failure, and testing time t: for the as-extruded condition, the final column identifies the specimen in Fig. 3. The two experimental conditions are considered separately in the following sections.

3.2.1. Cavitation in the annealed condition

The three sets of photomicrographs for the annealed condition represent essentially Region III, the transition from Region III to Region II, and the optimum superplastic condition in Region II, respectively.

Figs 4 and 5 show the fracture tip (Figs 4a and 5a) and an area away from the fracture tip (Figs 4b and 5b) for the specimens tested at initial strain rates of 3.3×10^{-2} and $1.3 \times 10^{-3}\,sec^{-1}$, respectively. In these and subsequent photomicrographs, the dark phase is the α-Al-rich phase, the light phase is the θ-$CuAl_2$ phase, and the tensile axis is horizontal.

Very few cavities were visible at the fracture tip of the specimen tested in Region III, as in Fig. 4a, and these cavities tended to be very near to the plane of failure and elongated along the tensile axis. The cavity density was extremely low at large distances from the fracture tip, as in Fig. 4b, and the few optically visible cavities were very small, isolated, and essentially rounded in appearance. This specimen failed through the development of a sharp neck so that cavitation appears to be of little significance under these conditions.

At the slower strain rate of $1.3 \times 10^{-3}\,sec^{-1}$, at the transition from Region III to Region II, there was a decrease in the severity of necking and a concomitant increase in the level of cavitation. There were many large cavities in the vicinity of the fracture tip, as shown in Fig. 5a, and these were elongated and

TABLE II Experimental conditions for photomicrographs of cavities

Region	Annealed condition			As-extruded condition			
	$\dot{\varepsilon}$ (sec^{-1})	$\Delta L/L_0$(%)	t (min)	$\dot{\varepsilon}$ (sec^{-1})	$\Delta L/L_0$(%)	t (min)	Specimen in Fig. 3
III	3.3×10^{-2}	160	0.8	3.3×10^{-2}	200	1	C
III → II	1.3×10^{-3}	265	33	6.7×10^{-4}	630	160	E
II	1.3×10^{-5}	1475	18 400	6.7×10^{-5}	1400	3500	G
II → I				1.3×10^{-5}	810	10 100	I

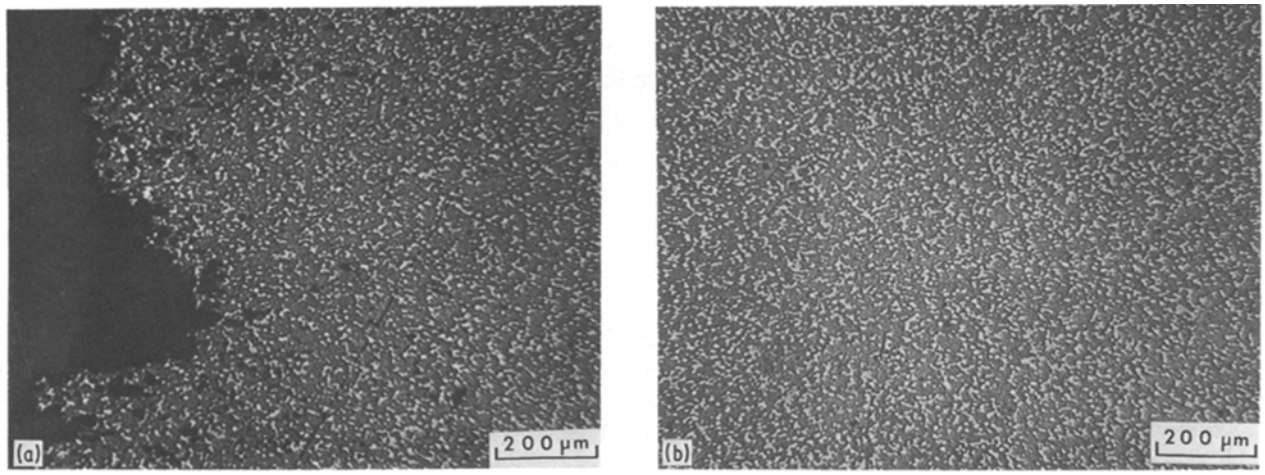

Figure 4 (a) Fracture tip and (b) area away from the fracture tip for an annealed specimen tested at an initial strain rate of $3.3 \times 10^{-2}\,sec^{-1}$.

interlinked primarily along the tensile axis but also, to a lesser extent, perpendicular to the stress axis. In general, cavities with radii $\leqslant 10\,\mu m$ were rounded in appearance, whereas the larger cavities were elongated in the tensile direction. Fig. 5b shows that there were also many isolated, and reasonably rounded, cavities at points remote from the fracture tip.

The annealed specimen tested at an initial strain rate of $1.3 \times 10^{-5}\,sec^{-1}$ exhibited the maximum recorded elongation of 1475%. This specimen pulled down to a fracture tip with a width of $\sim 550\,\mu m$ and inspection showed there was diffuse necking in the vicinity of the point of failure. Fig. 6a shows the fracture tip and an adjacent diffuse neck and Fig. 6b shows an area away from the fracture tip. There was extensive cavitation in this specimen under the condition of optimal superplasticity, and the degree of cavitation was especially pronounced in the region of diffuse necking as in Fig. 6a. This suggests that the failure mode under these conditions is intermediate between true superplasticity, in which the plastic flow is quasi-stable and the material pulls out to a point, and cavitation failure in which there is an absence of macroscopic necking and a fairly large cross-sectional area at the point of failure. The cavities in Fig. 6a are elongated and interlinked along the tensile axis, and there were also large, less elongated cavities away from the fracture tip as in Fig. 6b. Inspection suggested that the smaller cavities with radii $\leqslant 20\,\mu m$ were rounded whereas the larger cavities were elongated along the tensile axis. An examination of Fig. 6a reveals also a tendency for the cavities to form in stringers parallel to the tensile axis. Finally, a comparison of Figs 4, 5 and 6 indicates the occurrence of extensive grain growth at the slowest strain rate.

An examination of fractured specimens by scanning electron microscopy showed that the cavities tended to form preferentially on the α–θ interphase boundaries. An example is shown in Fig. 7 for the specimen tested at an initial strain rate of $1.3 \times 10^{-3}\,sec^{-1}$, where the α phase is dark and the θ phase is light. This observation confirms the earlier reports by Petty [6] and Bright *et al.* [14] on the Al–33% Cu eutectic alloy.

3.2.2. Cavitation in the as-extruded condition

As documented in Table II, the four sets of photomicrographs for the as-extruded condition represent essentially Region III, the transition from Region III to Region II, the optimum superplastic condition in Region II, and the transition from Region II to Region I, corresponding to the specimens labelled C, E, G and I in Fig. 3, respectively. Figs 8 to 11 show the fracture tip (Figs 8a to 11a) and an area away from the fracture tip (Figs 8b to 11b) for these four specimens.

Specimen C was tested at an initial strain rate of $3.3 \times 10^{-2}\,sec^{-1}$ and failed by necking. This specimen

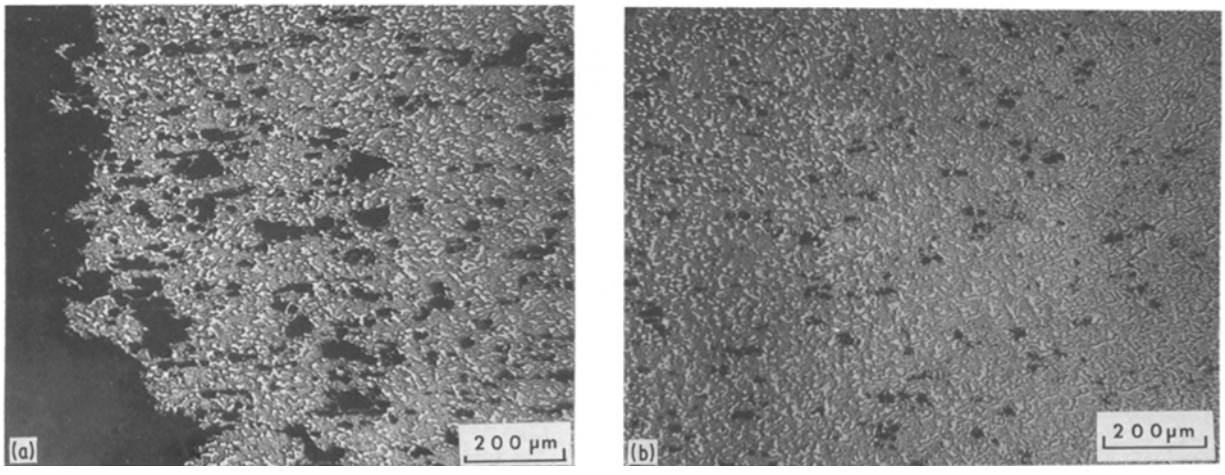

Figure 5 (a) Fracture tip and (b) area away from the fracture tip for an annealed specimen tested at an initial strain rate of $1.3 \times 10^{-3}\,sec^{-1}$.

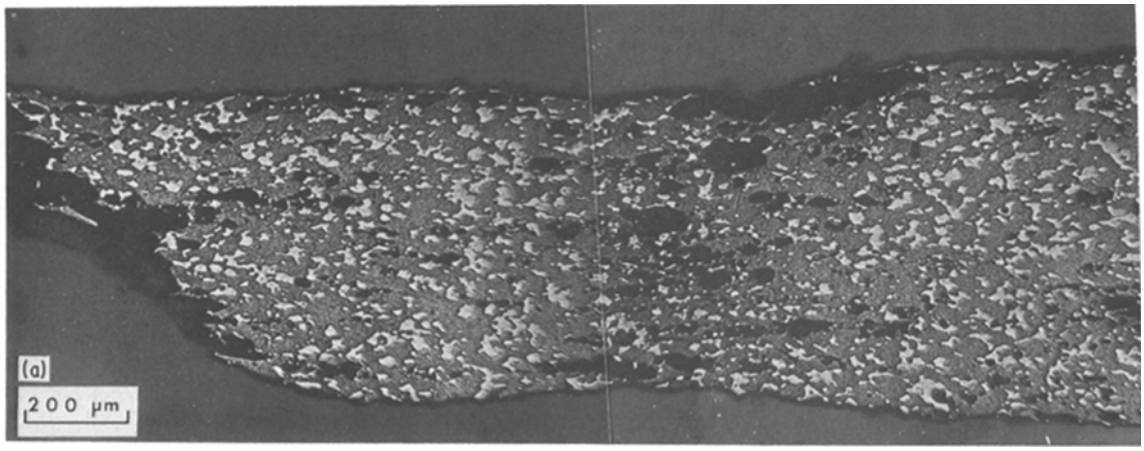

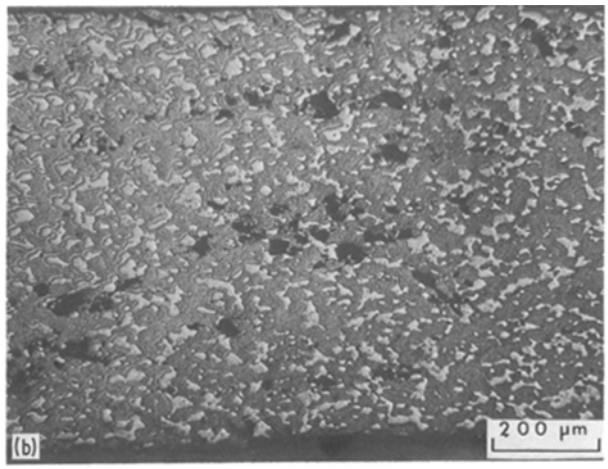

Figure 6 (a) Fracture tip and an adjacent diffuse neck and (b) area away from the fracture tip for an annealed specimen tested at an initial strain of $1.3 \times 10^{-5}\,\text{sec}^{-1}$.

contained many elongated cavities near the fracture tip and a low density of fairly large cavities away from the fracture tip, as shown in Fig. 8. This strain rate is the same as for Fig. 4 in the annealed condition, and it is apparent that the extent of cavitation is higher in the as-extruded condition. This is attributed to the larger elongation of 200% in the as-extruded material compared with 160% in the annealed material. In fact, the extent of cavitation in Fig. 8 is qualitatively intermediate between Figs 4 and 5 for annealed specimens fracturing at elongations of 160% and 265%, respectively.

Fig. 9 shows extensive cavitation in the specimen tested at an initial strain rate of $6.7 \times 10^{-4}\,\text{sec}^{-1}$, with large cavities elongated along the stress axis. There was some evidence for cavity interlinkage perpendicular to the stress axis under this testing condition, and Fig. 12 shows examples of interlinkage at A and two cavities very close to interlinkage at B.

The photomicrographs in Fig. 10 are for the optimum condition with an elongation to failure of 1400% at an initial strain rate of $6.7 \times 10^{-5}\,\text{sec}^{-1}$. There were many cavities in this condition, but interlinkage was almost exclusively along the tensile axis and there were many examples, as in Fig. 13, of adjacent elongated cavities separated by narrow ligaments of material.

Fig. 11 is for an initial strain rate of $1.3 \times 10^{-5}\,\text{sec}^{-1}$, where the specimen failed at an elongation of 810%. These photomicrographs provide clear evidence for the formation of cavities in stringers parallel to the tensile axis. The cavity morphology near to the fracture tip is similar to Fig. 10, although the total cavity density is probably higher due to the much longer testing time (~ 168 h for the specimen in Fig. 11). An important difference in this condition was the ability of some cavities to interlink perpendicular to the tensile axis, as shown in Fig. 11b.

As in the annealed condition, there was also evidence for grain growth at the lower strain rates. For example, measurements showed an average grain size at failure for Specimen G (Fig. 10) of $12.5 \pm 1.3\,\mu\text{m}$, representing growth by a factor of ~ 1.9.

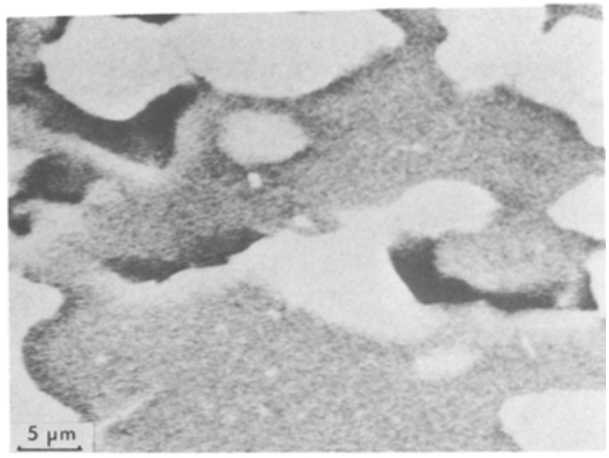

Figure 7 Preferential formation of cavities on α–θ interphase boundaries for an annealed specimen tested at an initial strain rate of $1.3 \times 10^{-3}\,\text{sec}^{-1}$.

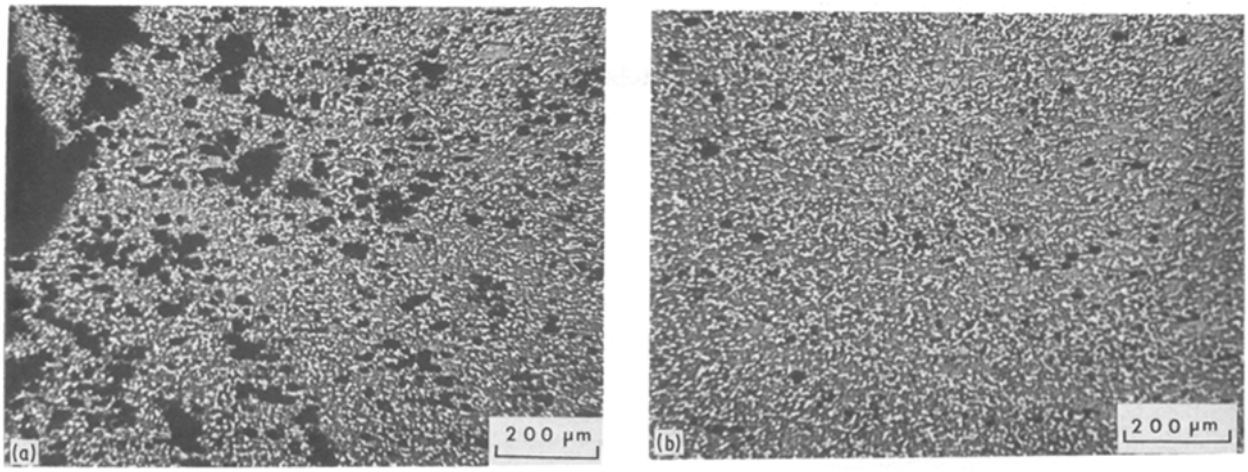

Figure 8 (a) Fracture tip and (b) area away from the fracture tip for an as-extruded specimen tested at an initial strain rate of $3.3 \times 10^{-2}\,sec^{-1}$.

4. Discussion

4.1. General observations on cavitation and fracture

Extensive cavitation was observed in this investigation in both the annealed and as-extruded material. In general, there appeared to be more cavitation in the as-extruded condition. At the fast initial strain rate of $3.3 \times 10^{-2}\,sec^{-1}$ (Figs 4 and 8), this difference may be due to the higher elongation in the as-extruded condition. However, this cannot account for the results at an initial strain rate of $1.3 \times 10^{-5}\,sec^{-1}$, where there was significantly more cavitation in the as-extruded material pulled to 810% (Fig. 11) than in the annealed material which failed at 1475% (Fig. 6). Livesey and Ridley [40] reported an increase in cavitation with increasing grain size in the Zn–22% Al eutectoid alloy, but this is not consistent with the present results where the as-extruded grain size (6.6 μm) is smaller than the annealed grain size (7.9 μm). The difference probably arises in the present investigation because of the stresses inherent in the as-extruded material from processing and also the relatively unstable nature of the grain configuration.

Kashyap and Tangri [29, 31] reported the occurrence of cavitation in the superplastic Al–33% Cu alloy, but, in contrast to the present results, they concluded that the degree of cavitation increases with increasing strain rate. While part of this discrepancy may be caused by the differences in strain level used to study cavitation in the two sets of experiments, it appears likely that the difference arises primarily because of the use of significantly different testing temperatures. Thus, Kashyap and Tangri [29, 31] examined cavitation at 813 K whereas the present results were obtained at 723 K. An increase in the testing temperature has two important effects, both of which will tend to decrease the extent of cavitation at the lower strain rates. First, the flow stress decreases with increasing temperature, and this leads to a decrease in the cavity nucleation rate, $\dot{N}$, as $\dot{N}$ is proportional to $\exp(-\gamma^3/\sigma_n^2 kT)$ where γ is the surface energy and σ_n is the local tensile stress acting across the boundary [41]. Second, the diffusional accommodation processes occur more rapidly at higher temperatures and this tends to attenuate the large stress concentrations caused by grain boundary sliding.

It was also observed in this investigation that most cavities were formed at the α–θ interphase boundaries, as shown in Fig. 7, and this is consistent with the early observations of Petty [6] and Bright *et al.* [14]. This is probably due to difficulties in accommodating sliding at the interphase boundaries, since it is known that sliding is an important deformation mode in superplasticity [42] and there are generally very significant

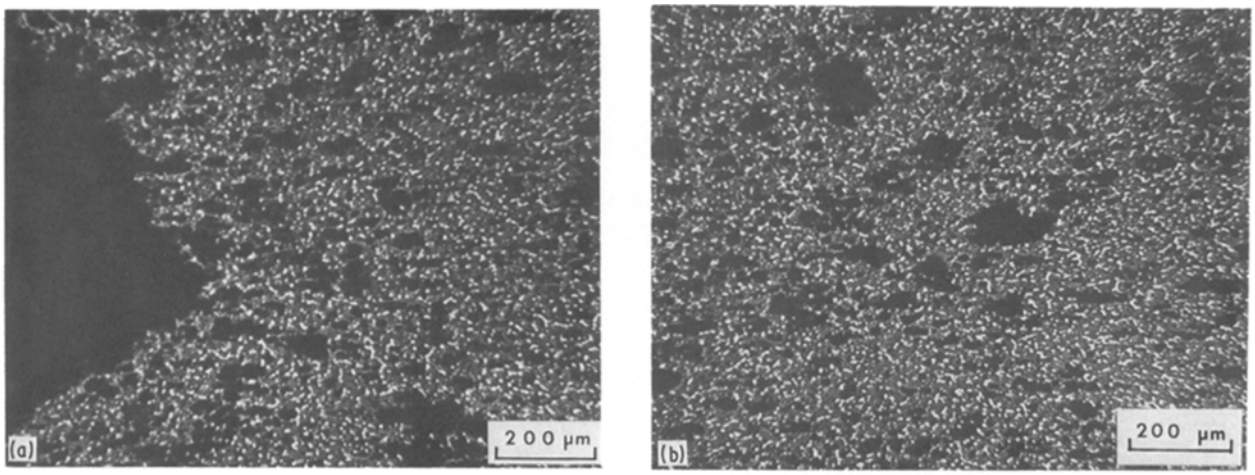

Figure 9 (a) Fracture tip and (b) area away from the fracture tip for an as-extruded specimen tested at an initial strain rate of $6.7 \times 10^{-4}\,sec^{-1}$.

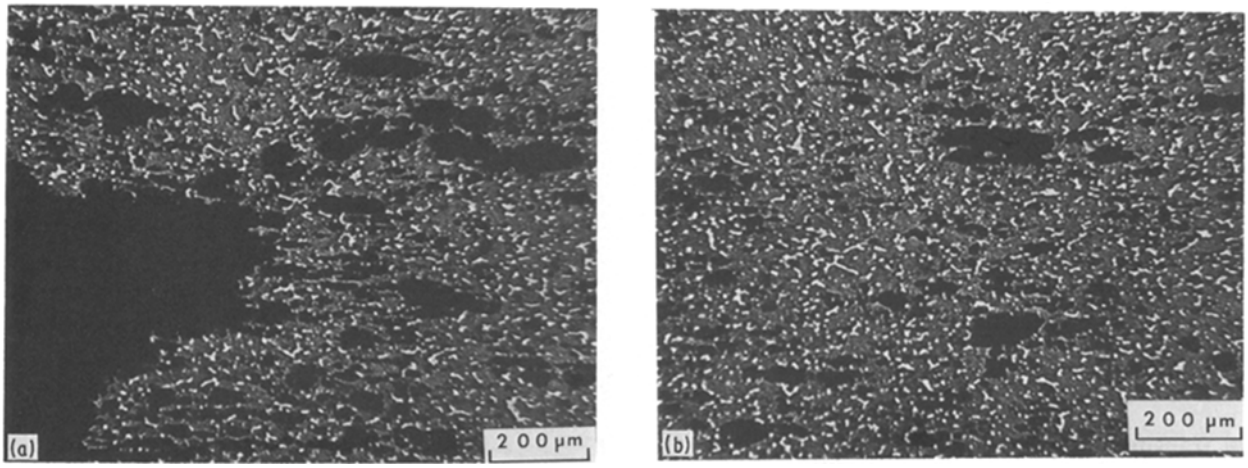

Figure 10 (a) Fracture tip and (b) area away from the fracture tip for an as-extruded specimen tested at an initial strain rate of 6.7×10^{-5} sec^{-1}.

differences in the amounts of sliding occurring at the three types of interface in two-phase superplastic alloys (for example, α–α, α–θ and θ–θ in Al–33% Cu) [43–46].

The alignment of cavities in stringers parallel to the tensile axis, as shown in Figs 6 and 11, is similar to the observations reported by Kashyap and Tangri [29, 31]. Detailed experimental studies in a superplastic commercial copper alloy have shown that the alignment of cavities in stringers is related to the alignment of coarse Co-rich particles along the rolling direction and the subsequent nucelation of cavities at these particles [47, 48]. It is important to note that microstructural examination by scanning electron microscopy failed to reveal the presence of coarse oxide particle stringers in the Al–Cu eutectic alloy used in this work. The present results, when examined in connection with an earlier report of cavitation in a high-purity superplastic Zn–22% Al alloy [49], suggest that coarse oxide particles are not necessary in order to develop cavitation in stringers parallel to the tensile axis.

The specimens in Fig. 3 show that the fracture behaviour depends on the strain rate. Necking occurs at the faster strain rates in Region III, but the severity of necking becomes less pronounced as the strain rate is reduced, and in the superplastic Region II the necking is very diffuse. The trend in necking is consistent with the anticipated behaviour based on the magnitude of the strain rate sensitivity, with the necking becoming less pronounced when the strain rate sensitivity is high [50]. The decrease in elongation to failure at the two lowest strain rates in Fig. 3, and the close similarity in appearance between Specimens F and H, provide additional support for the decrease in strain rate sensitivity at very low strain rates and the occurrence of a genuine Region I.

The occurrence of extensive cavitation very near to the fracture tip and markedly less cavitation at points remote from the fracture tip, as in Figs 5 and 8, suggests that cavitation is enhanced due to the higher local strains in the region of necking and/or by the triaxial state of stress in the necked region.

It is also interesting to note that, even under optimum superplastic conditions as for Specimen G in Fig. 3, the specimens do not pull out to a fine point at fracture. This suggests that the superplastic behaviour of the Al–33% Cu alloy is intermediate between the highly superplastic Pb–62% Sn [39] and Zn–22% Al [38] and the less superplastic commercial copper alloys such as CDA 638 [2, 51]. This is consistent with Fig. 6, which shows that the width of the fracture tip in Region II is neither as narrow as in Zn–22% Al

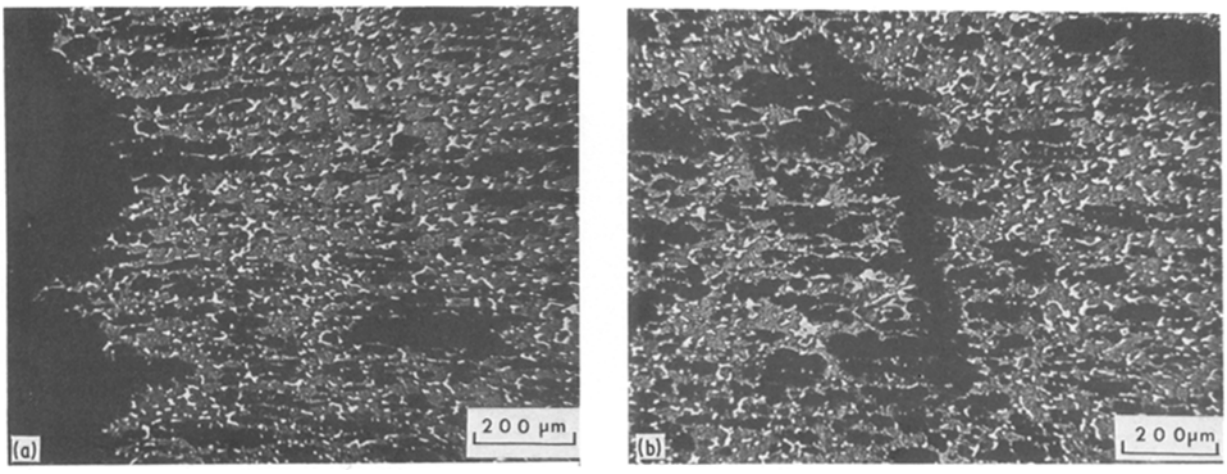

Figure 11 (a) Fracture tip and (b) area away from the fracture tip for an as-extruded specimen tested at an initial strain rate of 1.3×10^{-5} sec^{-1}.

where there is less cavitation [52] nor as broad as in CDA 638 where there is more cavitation [51].

4.2. An analysis of cavity growth

A general conclusion from this investigation was that the smaller cavities tended to be round and the larger cavities were usually elongated along the tensile axis. This is consistent with the general expectations from theories of cavity growth, since the cavities grow initially by diffusion and are approximately spherical but they grow subsequently by plastic flow in the surrounding material and become elongated [53]. There is a critical cavity radius which delineates the transition between these mechanisms [54, 55] and thereby predicts, on theoretical grounds, the transition from round to elongated cavities. It is appropriate, therefore, to apply this analysis to the present observations.

There are three distinct mechanisms of cavity growth in superplasticity. If a cavity is isolated on a single grain boundary and grows by absorbing vacancies which diffuse along the boundary, the growth rate is given by [56–58]

$$\frac{dr}{d\varepsilon} = \alpha\left(\frac{2\Omega\delta D_{gb}}{kT}\right)\left(\frac{1}{r^2}\right)\left(\frac{\sigma - (2\gamma/r)}{\dot{\varepsilon}}\right) \quad (1)$$

where r is the cavity radius, α is the cavity size-spacing parameter, Ω is the atomic volume, δ is the grain boundary width, D_{gb} is the coefficient of grain boundary diffusion, k is Boltzmann's constant and T is the absolute temperature.

For small and well separated cavities, the value of α is ~ 0.1 so that Equation 1 reduces to

$$\frac{dr}{d\varepsilon} = \left(\frac{\Omega\delta D_{gb}}{5kT}\right)\left(\frac{1}{r^2}\right)\left(\frac{\sigma - (2\gamma/r)}{\dot{\varepsilon}}\right) \quad (2)$$

A similar relationship was developed also by Dobeš and Čadek [59]. Equation 2 is the relationship for diffusion growth.

When the cavity is sufficiently large that it intersects, and absorbs vacancies from, a number of grain boundaries, the process is termed superplastic diffusion growth and the rate of growth is given by [60]

$$\frac{dr}{d\varepsilon} = \left(\frac{45\Omega\delta D_{gb}}{kT}\right)\left(\frac{1}{d^2}\right)\left(\frac{\sigma}{\dot{\varepsilon}}\right) \quad (3)$$

where d is the spatial grain size ($= 1.74\bar{L}$).

When the growth of the cavity is controlled by plastic flow in the surrounding material, the rate of growth is given by [61]

$$\frac{dr}{d\varepsilon} = r - \frac{3\gamma}{2\sigma} \quad (4)$$

Equation 4 is termed power-law growth.

The three growth mechanisms delineated by Equations 2 to 4 operate independently so that the fastest process is rate-controlling. The two diffusion processes, given by Equations 2 and 3, predict spherical cavities whereas the mechanism given by Equation 4 leads to the elongation of cavities along the stress axis. It is therefore a simple process to logarithmically plot $dr/d\varepsilon$ against r to predict the cavity radius associated with the change in cavity morphology from rounded to elongated.

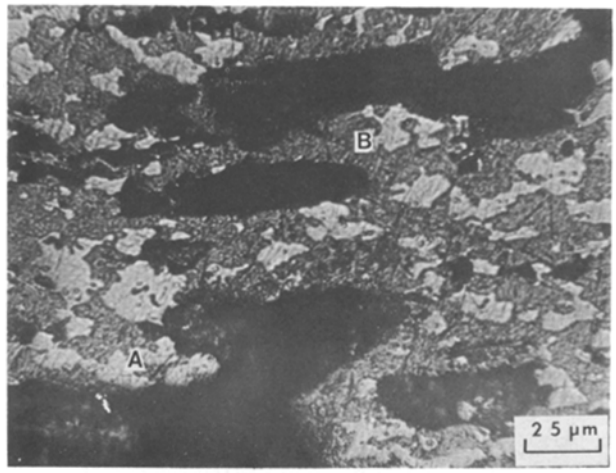

Figure 12 Cavity interlinkage (A) and two cavities very close to interlinkage (B) for an as-extruded specimen tested at an initial strain rate of $6.7 \times 10^{-4}\,sec^{-1}$.

In this investigation, cavities were observed predominantly on the α–θ interphase boundaries so that it is appropriate to use the interphase diffusion coefficient along the α–θ interface to evaluate Equations 2 and 3. From the experimental data of Ho and Weatherly [62], $D_{gb} = 0.11\exp(-97900RT)\,m^2\,sec^{-1}$, where R is the gas constant ($8.31\,J\,mol^{-1}\,K^{-1}$). Taking $\Omega = 1.1 \times 10^{-29}\,m^3$, $\delta = 10^{-9}\,m$ and $\gamma = 0.23\,J\,m^{-2}$ [62], the values of $dr/d\varepsilon$ were calculated using Equations 2 to 4 for the annealed grain size of $\bar{L} = 7.9\,\mu m$ and the two experimental conditions of $\dot{\varepsilon} = 1.3 \times 10^{-3}$ and $1.3 \times 10^{-5}\,sec^{-1}$, respectively: these strain rates correspond to the photomicrographs in Figs 5 and 6, respectively.

For these two strain rates, the calculations showed that superplastic diffusion growth, through Equation 3, made a negligible contribution to the overall cavity growth rate. The two other growth processes are illustrated in Fig. 14, and they show that the critical radius r_c, marking the transition from diffusion growth

Figure 13 Adjacent cavities separated by a narrow ligament for an as-extruded specimen tested at an initial strain rate of $6.7 \times 10^{-5}\,sec^{-1}$.

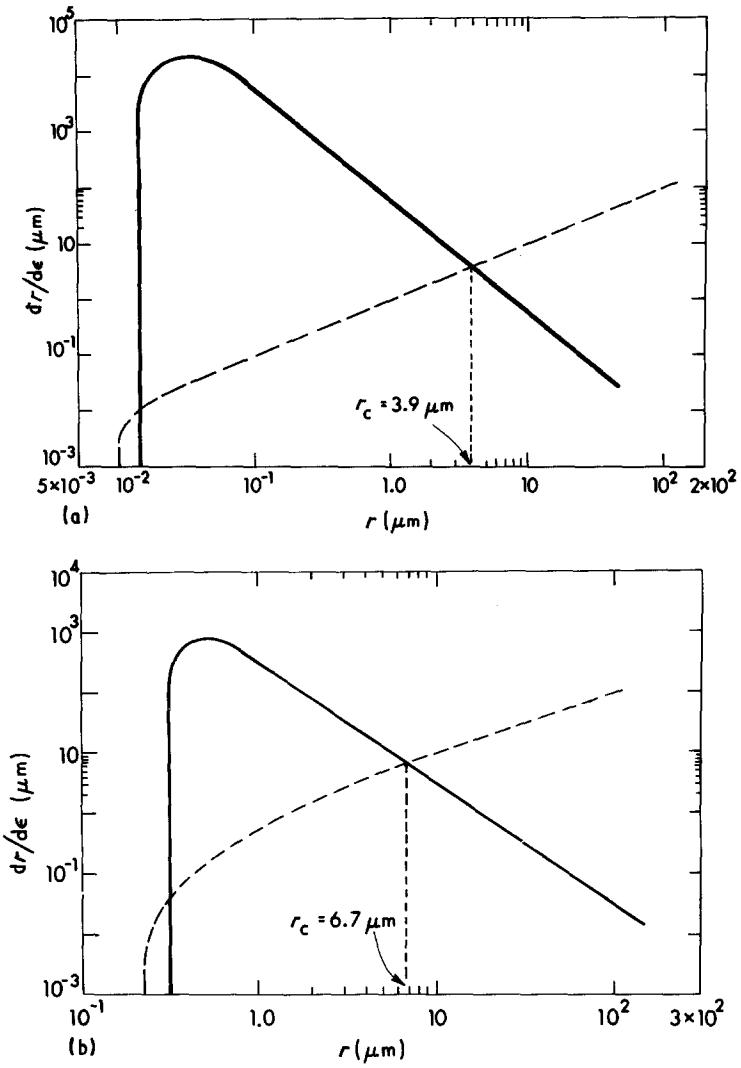

Figure 14 Cavity growth rate at 723 K against cavity radius for the annealed condition at initial strain rates of (a) $1.3 \times 10^{-3}\,sec^{-1}$ ($\sigma/\dot{\varepsilon} = 2.5 \times 10^4$ MPa sec) and (b) $1.3 \times 10^{-5}\,sec^{-1}$ ($\sigma/\dot{\varepsilon} = 1.2 \times 10^5$ MPa sec). (——) Diffusion growth, (– – –) power-law growth.

to power-law growth, occurs at cavity radii of 3.9 and 6.7 μm for the two experimental conditions, respectively.

It was noted earlier that the transition from rounded to elongated cavities occurred at cavity radii of the order of ~ 10 and $\sim 20\,\mu$m for Figs 5 and 6, respectively. These values are consistent with the calculations in Fig. 14 to within a factor of < 3. As noted elsewhere [63], there is a tendency for surface diffusion to spheroidize elongated cavities at elevated testing temperatures, so that the observed agreement between the theoretical and experimental results is reasonable.

Finally, it is interesting to note, from inspection of Fig. 14, that a decrease in the initial strain rate by two orders of magnitude leads to an increase in the value of r_c by less than a factor of two. This is because, by equating Equations 2 and 4, the critical radius is given by [54, 55]

$$r_c = \left(\frac{\Omega\delta D_{gb}}{5kT}\right)^{1/3}\left(\frac{\sigma}{\dot{\varepsilon}}\right)^{1/3} \quad (5)$$

so that, at a constant temperature, r_c is determined exclusively by the magnitude of $\sigma/\dot{\varepsilon}$. As indicated in Fig. 14, the values of $\sigma/\dot{\varepsilon}$ change only from 2.5×10^4 to 1.2×10^5 MPa sec for the two selected conditions, and this relatively small change is due to the high strain rate sensitivity of $m \simeq 0.7$ in Region II in the annealed condition (Fig. 1).

5. Summary and conclusions

1. The Al–33% Cu eutectic alloy was tested in both an annealed and an as-extruded condition. For both conditions, there is a sigmoidal relationship between flow stress and strain rate with maximum ductilities occurring at intermediate strain rates in Region II where the strain rate sensitivity is also a maximum.

2. Necking occurs at the faster strain rates in Region III, but the severity of necking becomes less pronounced with decreasing strain rate and the necks are very diffuse in Region II.

3. Inspection of fractured specimens showed the occurrence of extensive cavitation, especially at the lower strain rates. In general, cavitation was more pronounced near to the fracture tip, and there appeared also to be more cavitation in the as-extruded condition.

4. It was observed that cavities form preferentially on the α–θ interphase boundaries.

5. Using the coefficient for interphase diffusion along the α–θ interface, it is shown that the observed change in cavity morphology, from small rounded cavities to large cavities elongated along the tensile axis, is reasonably consistent with the theories of cavity growth.

Acknowledgement

This work was supported in part by the National Science Foundation under Grant No. DMR-8503224.

References

1. R. H. JOHNSON, *Metall. Rev.* **15** (1970) 115.
2. T. G. LANGDON, *Met. Sci.* **16** (1982) 175.
3. A. A. PRESNYAKOV and V. V. CHERVYAKOVA, *Izvest. Akad. Nauk SSSR, Otdel. Tekh. Nauk* No. 1 (1958) 120.
4. *Idem, Vestnik Akad. Nauk Kazakh SSR* **14** (12) (1958) 76.
5. *Idem, Fiz. Metal. Metalloved.* **8** (1) (1959) 114.
6. E. R. PETTY, *J. Int. Metals* **91** (1962–63) 274.
7. D. L. HOLT and W. A. BACKOFEN, *Trans. ASM* **59** (1966) 755.
8. M. J. STOWELL, J. L. ROBERTSON and B. M. WATTS, *Met. Sci. J.* **3** (1969) 41.
9. B. M. WATTS and M. J. STOWELL, *J. Mater. Sci.* **6** (1971) 228.
10. R. D. SCHMIDT-WHITLEY, *Z. Metallkde* **64** (1973) 552.
11. S. HORI and N. FURUSHIRO, *Tech. Rpts Osaka Univ.* **23** (1973) 75.
12. C. P. CUTLER, J. W. EDINGTON, J. S. KALLEND and K. H. MELTON, *Acta Metall.* **22** (1974) 665.
13. G. RAI and N. J. GRANT, *Metall. Trans A* **6A** (1975) 385.
14. M. W. A. BRIGHT, D. M. R. TAPLIN and H. W. KERR, *J. Engng Mater. Tech.* **97** (1975) 1.
15. T. HATAYAMA and O. IZUMI, *J. Jpn Soc. Tech. Plasticity* **16** (1975) 981.
16. S. HORI, N. FURUSHIRO and S. KAWAGUCHI, *J. Jpn Inst. Light Metals* **25** (1975) 361.
17. *Idem,* in Proceedings of 19th Japan Congress on Materials Research (Society of Materials Science, Kyoto, 1976) p. 1.
18. K. A. PADMANABHAN and G. J. DAVIES, *Met. Sci.* **11** (1977) 177.
19. Y. KOBAYASHI, Y. ISHIDA and M. KATO, *Scripta Metall.* **11** (1977) 51.
20. N. FURUSHIRO and S. HORI, *ibid.* **12** (1978) 35.
21. K. MATSUKI, K. MINAMI, M. TOKIZAWA and Y. MURAKAMI, *Met. Sci.* **13** (1979) 619.
22. T. HATAYAMA and O. IZUMI, *J. Jpn Inst. Metals* **45** (1981) 1326.
23. G. A. NASSEF, M. SUÉRY and A. EL-ASHRAM, *Met. Tech.* **9** (1982) 355.
24. T. HATAYAMA, T. OKABE, H. TAKEI and Y. HODO, *J. Jpn Inst. Metals* **46** (1982) 205.
25. T. OKABE, T. HATAYAMA and H. TAKEI, *ibid.* **46** (1982) 211.
26. G. A. NASSEF and M. SUÉRY, *J. Mater. Sci.* **18** (1983) 3031.
27. G. RAI and N. J. GRANT, *Metall. Trans. A* **14A** (1983) 1451.
28. B. P. KASHYAP and K. TANGRI, *Scripta Metall.* **19** (1985) 1419.
29. *Idem, ibid.* **20** (1986) 769.
30. T. HATAYAMA, T. OKABE and H. TAKEI, *Trans. Jpn Inst. Metals* **27** (1986) 576.
31. B. P. KASHYAP and K. TANGRI, *Metall. Trans. A* **18A** (1987) 417.
32. A. H. CHOKSHI and T. G. LANGDON, *Scripta Metall.* **21** (1987) 1669.
33. *Idem, Metall. Trans. A* (in press).
34. *Idem, Mater. Sci. Tech.* (press).
35. D. A. WOODFORD, *Trans. ASM* **62** (1969) 291.
36. E. W. HART, *Acta. Metall.* **15** (1967) 351.
37. F. A. NICHOLS, *ibid.* **28** (1980) 663.
38. F. A. MOHAMED, M. M. I. AHMED and T. G. LANGDON, *Metall. Trans. A* **8A** (1977) 933.
39. M. M. I. AHMED and T. G. LANGDON, *ibid.* **8A** (1977) 1832.
40. D. W. LIVESEY and N. RIDLEY, *J. Mater. Sci.* **17** (1982) 2257.
41. R. RAJ and M. F. ASHBY, *Acta Metall.* **23** (1975) 653.
42. T. G. LANGDON, *J. Mater. Sci.* **16** (1981) 2613.
43. T. CHANDRA, J. J. JONAS and D. M. R. TAPLIN, *ibid.* **13** (1978) 2380.
44. R. B. VASTAVA and T. G. LANGDON, *Acta. Metall.* **27** (1979) 251.
45. P. SHARIAT, R. B. VASTAVA and T. G. LANGDON, *ibid.* **30** (1982) 285.
46. Z.-R. LIN, A. H. CHOKSHI and T. G. LANGDON, *J. Mater. Sci.* in press.
47. C. H. CÁCERES and D. S. WILKINSON, *Acta Metall.* **32** (1984) 423.
48. A. H. CHOKSHI, *Metall. Trans. A* **18A** (1987) 63.
49. D. A. MILLER and T. G. LANGDON, *ibid.* **9A** (1978) 1688.
50. F. A. MOHAMED and T. G. LANGDON, *Acta Metall.* **29** (1981) 911.
51. S.-A. SHEI and T. G. LANGDON, *J. Mater. Sci.* **13** (1978) 1084.
52. M. M. I. AHMED, F. A. MOHAMED and T. G. LANGDON, *ibid.* **14** (1979) 2913.
53. D. A. MILLER and T. G. LANGDON, *Metall. Trans. A* **10A** (1979) 1869.
54. *Idem, Scripta Metall.* **14** (1980) 179.
55. A. H. CHOKSHI, *J. Mater. Sci.* **21** (1986) 2073.
56. D. HULL and D. E. RIMMER, *Phil. Mag.* **4** (1959) 673.
57. M. V. SPEIGHT and W. BEERÉ, *Met. Sci.* **9** (1975) 190.
58. W. BEERÉ and M. V. SPEIGHT, *ibid.* **12** (1978) 172.
59. F. DOBEŠ and J. ČADEK, *Scripta Metall.* **4** (1970) 1005.
60. A. H. CHOKSHI and T. G. LANGDON, *Acta Metall.* **35** (1987) 1089.
61. J. W. HANCOCK, *Met. Sci.* **10** (1976) 319.
62. E. HO and G. C. WEATHERLY, *Acta Metall.* **23** (1975) 1451.
63. A. H. CHOKSHI and A. K. MUKHERJEE, *Mater. Sci. Engng*, in press.

Received 9 November 1987
and accepted 1 March 1988